

# Fast Numerical Upscaling of Heat Equation for Fibrous Materials

Oleg Iliev · Raytcho Lazarov · Joerg Willems

April 6, 2009

*Dedicated to the memory of Richard E. Ewing*

**Abstract** We are interested in numerical methods for computing the effective heat conductivity of fibrous insulation materials, such as glass or mineral wool, characterized by low solid volume fractions and high contrasts, i.e. high ratios between the thermal conductivities of the fibers and the surrounding air. We consider a fast numerical method for solving some auxiliary cell problems appearing in this upscaling procedure. The auxiliary problems are boundary value problems of the steady-state heat equation in a representative elementary volume occupied by fibers and air. We make a simplification by replacing these problems with appropriate boundary value problems in the domain occupied by the fibers only. This common approach in the engineering practice has been theoretically justified for high contrast materials in a recent paper to which the authors contributed. Finally, the obtained problems are further simplified by taking advantage of the slender shape of the fibers and assuming that they form a network. A discretization on the graph defined by the fibers is presented and error estimates are provided. The resulting algorithm is discussed and the accuracy and the performance of the method are illustrated on a number of numerical experiments.

*Keywords:* effective heat conductivity, numerical upscaling, fibrous materials.

## 1 Introduction

A wide class of insulation materials, such as glass and mineral wool, fiber reinforced composites, etc., are composed of, or include, a large number of fibers. These materials are characterized by very low volume fractions and much higher conductivities of the fibrous materials compared with the surrounding air in the insulation materials, or compared with the bulk material in composite materials. In [6], it was shown that the effective heat conductivities of composite materials containing networks of highly conductive materials can be computed approximately by solving sets of auxiliary boundary value problems on the highly conductive path-connected components only. Using this result, we propose a fast method for computing the effective thermal conductivities of fibrous materials by integrating over those parts occupied by the fibers only. The computational domain is a graph of the interconnected fibers with intersection points of the fibers being nodes of the graphs. Thus, the problem for upscaling the conductivities of fibrous materials reduces to solving Laplace's equation on a graph.

---

O. Iliev

Fraunhofer Institut für Techno- und Wirtschaftsmathematik, Fraunhofer-Platz 1, 67663 Kaiserslautern, Germany  
and Institute of Mathematics, Bulgarian Academy of Science, Acad. G.Bonchev str., bl.8, 1113 Sofia, Bulgaria  
E-mail: oleg.iliev@itwm.fraunhofer.de

R. Lazarov

Department of Mathematics Texas A&M University College Station, TX, 77843, USA E-mail:  
lazarov@math.tamu.edu

J. Willems

Fraunhofer Institut für Techno- und Wirtschaftsmathematik, Fraunhofer-Platz 1, 67663 Kaiserslautern, Germany  
E-mail: joerg.willems@fraunhofer.itwm.fhg.de

Recalling homogenization theory (cf. [2, 10, 14, 18] and the references therein) the effective properties of heterogeneous materials can be calculated by solving suitable sets of “cell problems” on a representative elementary volume (REV). The equation under consideration in this paper is the stationary heat equation in a REV,  $\Omega^H \subset \mathbb{R}^3$ , a cube with side-length  $H$  and faces parallel to the coordinate planes. We rescale the REV by  $1/H$ , so after that the domain, denoted by  $\Omega$ , is the unit cube  $(0, 1)^3$ . Let  $\Omega_M$  and  $\Omega_A$  be two open sets such that  $\overline{\Omega}_M \cup \overline{\Omega}_A = \overline{\Omega}$  and satisfying some mild regularity assumptions described in [6]. We think of  $\Omega_M$  and  $\Omega_A$  being the highly (metal, glass) and lowly (air) conductive parts of  $\Omega$ , respectively.

According to [8, 10, 14, 18], the solutions  $u_i$ ,  $i = 1, 2, 3$  of the boundary value problems

$$\begin{aligned} \nabla \cdot (K \nabla u_i) &= 0 && \text{in } \Omega, \\ u_i &= x_i && \text{on } \partial\Omega, \end{aligned} \quad (1)$$

with

$$K(\mathbf{x}) = \begin{cases} K_A & \text{for } \mathbf{x} \in \Omega_A, \\ K_M & \text{for } \mathbf{x} \in \Omega_M, \end{cases}$$

can be used to obtain the effective thermal conductivity tensor  $\tilde{K}$  of the material  $\Omega$  by the formula

$$\tilde{K}\mathbf{e}_i = \langle K \nabla u_i \rangle_\Omega, \quad \text{where} \quad \langle \cdot \rangle_\Omega := \frac{1}{|\Omega|} \int_\Omega \cdot d\mathbf{x}. \quad (2)$$

Here  $|\cdot|$  denotes the Lebesgue measure and  $\mathbf{e}_i \in R^3$  is the  $i$ -th unit vector, so that  $\tilde{K}\mathbf{e}_i$  is the  $i$ -th column of  $\tilde{K}$ . We further assume that  $K_M = 1$  and  $K_A = \delta$  with  $\delta \ll 1$ . This means that the fibers have a constant conductivity which is much higher than the conductivity of the surrounding air. We refer to this large difference as high contrast. For this case it was shown in [6] that

$$\tilde{K}\mathbf{e}_i = \frac{1}{|\Omega|} \int_{\Omega_M} K \nabla v_i + \mathcal{O}(\delta), \quad i = 1, 2, 3, \quad (3)$$

where  $v_i$  is the solution of the following constant coefficient problem

$$\begin{cases} \Delta v_i = 0 & \text{in } \Omega_M, \\ \nabla v_i \cdot \mathbf{n} = 0 & \text{on } \partial\Omega_M \setminus \partial\Omega, \\ v_i = x_i & \text{on } \partial\Omega \cap \partial\Omega_M, \end{cases} \quad (4)$$

with  $\Delta$  being the Laplace operator and  $\mathbf{n}$  the outer unit normal vector to the boundary of  $\partial\Omega_M$ . Note,  $v_i$  is a harmonic function in the subdomain  $\Omega_M$  occupied by the fibers. Here we assume, that all path-connected components of  $\Omega_M$  intersect  $\partial\Omega$ . According to [6] this assumption is quite reasonable, since we may disregard those path-connected components of  $\Omega_M$  that do not touch the boundary. The method we propose and study in this paper is a further simplification of the method described in [6] and specializes on fibrous materials. We also remark that in the production process of these materials one frequently adds some binder material that is deposited on the fibers (see Figure 1) and is usually applied to provide better mechanical properties of the insulation fibrous material.

Methods, for computing the effective properties of composite materials based on solving problems in the highly conductive subdomains only, have been used previously by engineers and physicists (cf. e.g. [1, pp. 105–106]). It should be noted that many other practical problems are described by mathematical problem (1). For example, a method for calculating the permeability of fractured porous media, suggested by Barenblatt in the 1960s, is based on computing the flow in the fractures and neglecting the flow through the remaining lowly permeable part of the media. This approach is widely used in a number of applications in geoscience.

Recently, in [15, 16], a similar approach was used to compute the effective conductivity of fibrous porous media in the cases of perfect, weak, and imperfect contacts between the fibers. In the case of perfect contact, the discretization used in [15, 16] is essentially the same as the one in the paper at hand. In this respect the ideas of this paper are well established. We, however, derive the discretization in a rigorous mathematical way, study its properties such as stability and symmetry, and discuss and study experimentally the behavior with respect to the small parameters, the fiber diameters and the fiber lengths.

Often, the influence of the lowly conductive material is not taken into account in computing the effective properties of the media (see, e.g. [1], [15], [16]). Accounting for it can, however, be essential for the accurate calculation of effective thermal conductivities. This is especially pronounced for materials with very low solid volume fractions, a representative case for many industrial insulation materials. We adopt the inexpensive way described in [6] of taking into account these contributions.

The properties of fibrous materials have been subject to intensive studies in homogenization theory (see, e.g. [4,5,11]). In [5], elliptic equations on various lattice structures with homogeneous Neumann boundary conditions on the interfaces were used in deriving effective material properties. This setting is very similar to problem (4). The objectives in [4,5,11], however, are to get analytical results for periodic trust-like structures as the period and the diameter of the rods tend to zero.

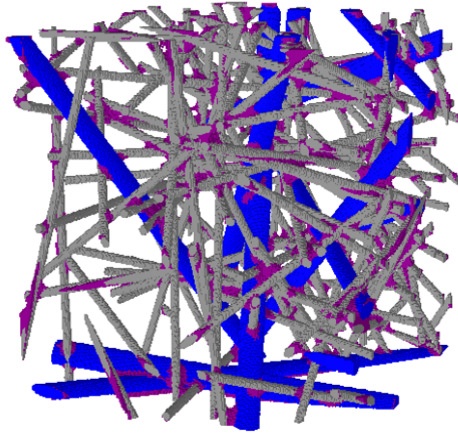


**Fig. 1** 3-dimensional fiber structure with binder material.

a large enough volume. Due to the rescaling, the characteristic parameters, specified in Assumption 1 and used in the convergence analysis, tend to zero as the size of the volume grows, i.e. when the media become statistically homogeneous and effective conductivities exist.

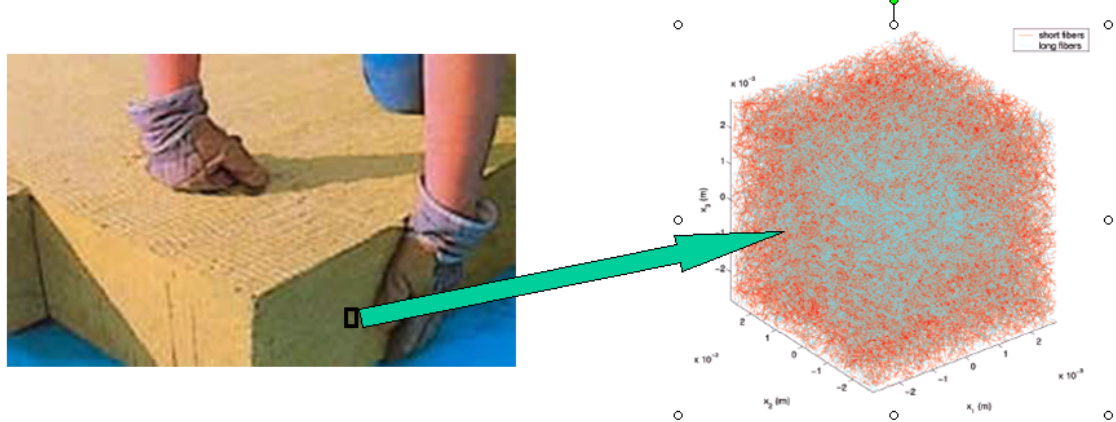


**Fig. 2** Taking a small sample of a fibrous structure.

The remainder of the paper is organized as follows: In Section 2 we introduce the necessary notations and definitions as well as some related assumptions. In Section 3 we discuss a finite volume discretization over the 3-dimensional graph formed by the fibers (done in the style of the monographs [7,12]). In particular, we show that the derived discretization yields a system of equations for the unknown temperatures at the mesh points with a symmetric and positive definite matrix. Further, a detailed analysis of the dependence of the discretization error on the fiber diameters and lengths is presented. Section 4 provides conclusions and results from numerical simulations for a number of applied engineering problems demonstrating the

We focus on fast numerical computations for random fibrous structures. More precisely, the aim of this paper is to derive, analyze, and justify an algorithm for the approximation of effective thermal conductivities of large sparse high-contrast fibrous materials (cf. Figure 1). In particular, we study the properties of this algorithm with respect to two characteristic parameters related to the fiber diameters and the distances between fiber intersections (see Assumption 1).

Recalling that effective properties can only be introduced for REVs, one can think of the following procedure: For an arbitrary point in the fibrous media one may consider a sequence of volumes centered at this point of increasing sizes (see Figures 2 and 3). Solving the (rescaled) cell problem (1) in each of the volumes and calculating the respective functional given by (2), one can find out when the effective conductivity stabilizes and therefore the corresponding volumes can be considered representative. This means that the calculated value has a meaning of an effective conductivity at the center point only for

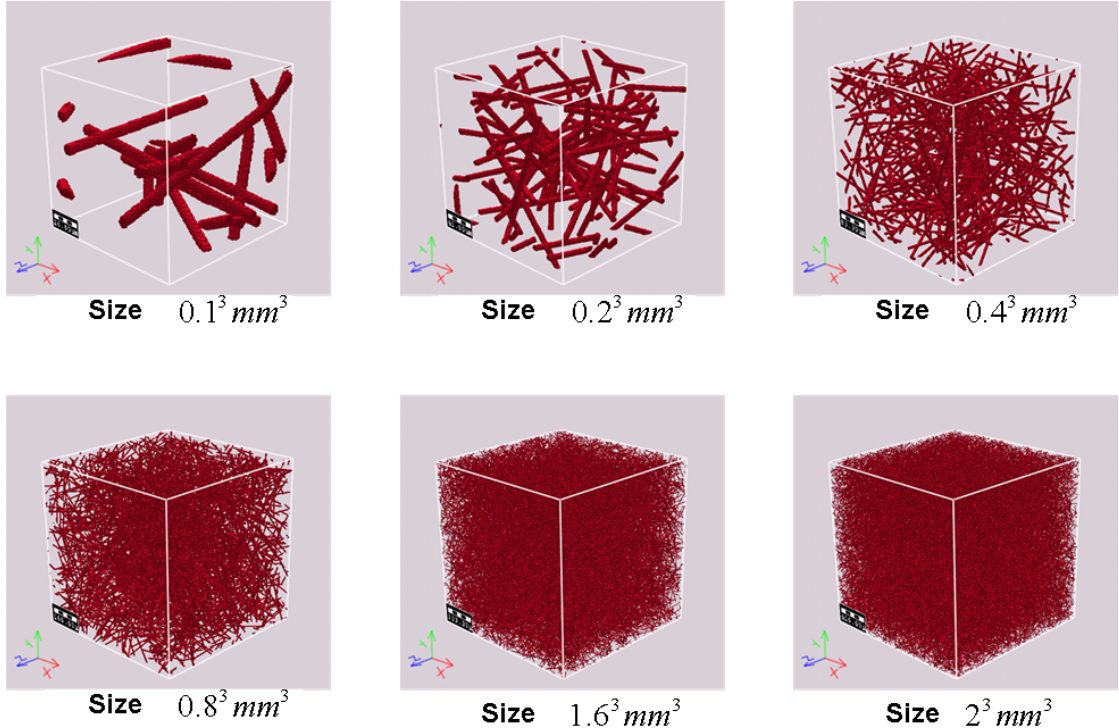


**Fig. 3** Increasingly larger sample volumes around the same center point.

accuracy and efficiency of our algorithm by comparing its performance with numerical results produced by other methods.

## 2 Notation and Definitions

By a fiber we mean a cylindrical object of finite length. We assume that the axis of this cylinder is a straight line. A generalization to curvilinear fibers is straightforward (cf. [5]). Furthermore, the length of a fiber is assumed to be much larger than its diameter (see Assumption 1). To generate a fibrous geometry these objects are randomly “thrown into”  $\Omega$  and cut-off at the boundary  $\partial\Omega$ . The set of all intersections of the cylinder axes with  $\partial\Omega$  is denoted by  $\partial\omega$ . The actual numerical generation of our fibrous geometries is done by GeoDict<sup>1</sup>. With this random construction different fibers may and, in general, will intersect. Now, let  $\omega$  be the set of points, where two or more fibers cross. To avoid unnecessary technicalities, we assume, that whenever two fibers (i.e. the cylindrical objects) have a nonempty intersection the same holds true for their axes. For more general models of interaction through the surfaces of intersecting fibers we refer to [15] and [16]. We also define  $\bar{\omega} := \omega \cup \partial\omega$ , and we assume that all nodes in  $\bar{\omega}$  are numbered in some way.

The (circular) cross-section of a fiber perpendicular to its axis and in the middle of two nodes from  $\bar{\omega}$  being adjacent on that fiber is denoted by  $S$ . For each cross-section  $S$  we denote the center of mass by  $\mathbf{x}_S := \int_S \xi dS(\xi)/|S|$ . The set of all points  $\mathbf{x}_S$  on cross-sections between two nodes is denoted by  $\mathcal{S}$ . For  $\mathbf{x}_S \in \mathcal{S}$  we denote by  $\mathbf{x}_S^+ \in \bar{\omega}$  and  $\mathbf{x}_S^- \in \bar{\omega}$  the higher and lower numbered node adjacent (on the fiber) to  $\mathbf{x}_S$ , respectively. For an illustration of the above definitions we refer to Figure 4.

Further, we need a notion of characteristic distance  $h$  between two adjacent (i.e. adjacent on a fiber) nodes and characteristic diameter  $d$  of all fibers in  $\bar{\Omega}$ . More precisely, we make the following

**Assumption 1** (a) There exist two parameters,  $h, d \in \mathbb{R}$  and two constants,  $c_{h,d}, C_{h,d} \in \mathbb{R}$ , all independent of  $H$ , such that for all cross-sections  $S$  with  $\mathbf{x}_S \in \mathcal{S}$

$$c_{h,d}h \leq \|\mathbf{x}_S^+ - \mathbf{x}_S^-\|_2 \leq C_{h,d}h \quad \text{and} \quad c_{h,d}d \leq \text{diam}(S) \leq C_{h,d}d. \quad (5)$$

<sup>1</sup> See [www.geodict.com](http://www.geodict.com) for more information about this software.

with  $\|\cdot\|_2$  denoting the standard Euclidean norm in  $\mathbb{R}^3$ .

(b)  $d \ll h \ll 1$ .

We refer to  $h$  and  $d$  as characteristic distance between nodes and characteristic fiber diameter, respectively. Assumption 1 is necessary in order to have a meaningful notion of a graph induced by the fibers (the edges of the graph) and their intersections (the nodes of the graph). For a sufficiently large sample size the scaling by  $H$ , cf. (1), gives the quantities  $h$  and  $d$  a meaning of small parameters. Thus,  $h$  is the “microscopic” characteristic length of the physics, i.e. the length upon which microscopic temperature gradients occur.

For each node  $\mathbf{x} \in \bar{\omega}$  we define  $V_{\mathbf{x}}$  to be the volume, consisting of all fiber-segments surrounding  $\mathbf{x}$  and bounded by the cross-sections  $S$  adjacent to  $\mathbf{x}$ . The numbering of  $\bar{\omega}$  induces a corresponding numbering on the volumes  $V_{\mathbf{x}}$ . With this we define  $\mathbf{n}_S^\mp$  to be the unit normal vector to  $S$  pointing from the lower to the higher numbered volume (see Figure 6(a)). Furthermore, for  $\mathbf{x} \in \bar{\omega}$  we set  $\mathcal{S}_{\mathbf{x}}$  to be those points in  $\mathcal{S}$  which lie on the boundary of  $V_{\mathbf{x}}$ , i.e.  $\mathcal{S}_{\mathbf{x}} := \partial V_{\mathbf{x}} \cap \mathcal{S}$ . For each  $\mathbf{x}_S \in \mathcal{S}$  we define  $V_S$  to be the cylindrical volume between two adjacent nodes from  $\bar{\omega}$ , such that  $S$  is contained in the enclosed volume, see Figure 6(a). Note, that near  $\mathbf{x} \in \omega$  the volumes  $V_S$  for different  $\mathbf{x}_S \in \mathcal{S}$  actually overlap. These overlapping regions, however, only have a volume that is  $\mathcal{O}(d^3)$ . The same estimate holds true for the volumes close to  $\mathbf{x} \in \partial\omega$ , which belong to the fiber but not  $V_S$  and vice versa (see Figure 6(b)).

For a very regular fiber arrangement depicted in Figure 5 we see, that

$$\#\bar{\omega} = \mathcal{O}\left(\frac{1}{h^3}\right). \quad (6)$$

As indicated in Section 1, some binder material is applied in the production process of glass and mineral wool. For simplicity the thermal conductivity of this binder material is assumed to be equal to that of the fibers. Figures 1 and 6(b) show how this binder can be deposited at the fibers. Combining the last two observations we make the following

**Assumption 2** Estimate (6) holds for our general fibrous geometries. Furthermore, the volume of each binder segment is  $\mathcal{O}(d^3)$ , and as for the fiber crossings we have  $\mathcal{O}(\frac{1}{h^3})$  of these segments.

Due to the binder segments the boundary of  $\Omega_M$  has no re-entrant corners, and thus the solution of (4) is regular enough to carry out the analysis below.

Now, we introduce the following sets of grid functions, defined on  $\bar{\omega}$  and  $\mathcal{S}$ , respectively.

### Definition 1

$$\mathcal{U} := \{y : \bar{\omega} \rightarrow \mathbb{R}\}, \quad \mathcal{F} := \{\chi : \mathcal{S} \rightarrow \mathbb{R}^3\}.$$

Now we introduce some difference operators and scalar products on the unstructured grids  $\bar{\omega}$  and  $\mathcal{S}$ . We define difference operators  $\mathcal{G}$ , the discrete gradient, and  $\mathcal{D}$ , the discrete divergence, corresponding to the differential operators  $\nabla$  and  $\nabla \cdot$ , respectively.

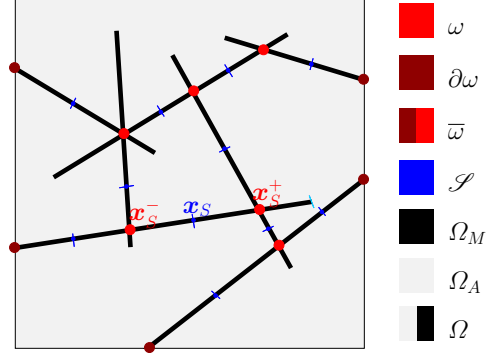


Fig. 4 Domain with nodes and cross-sections.

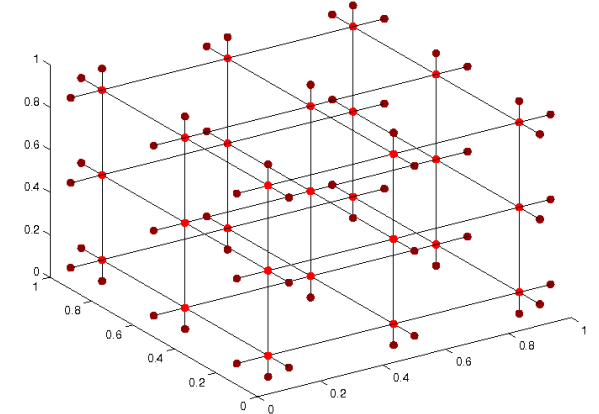
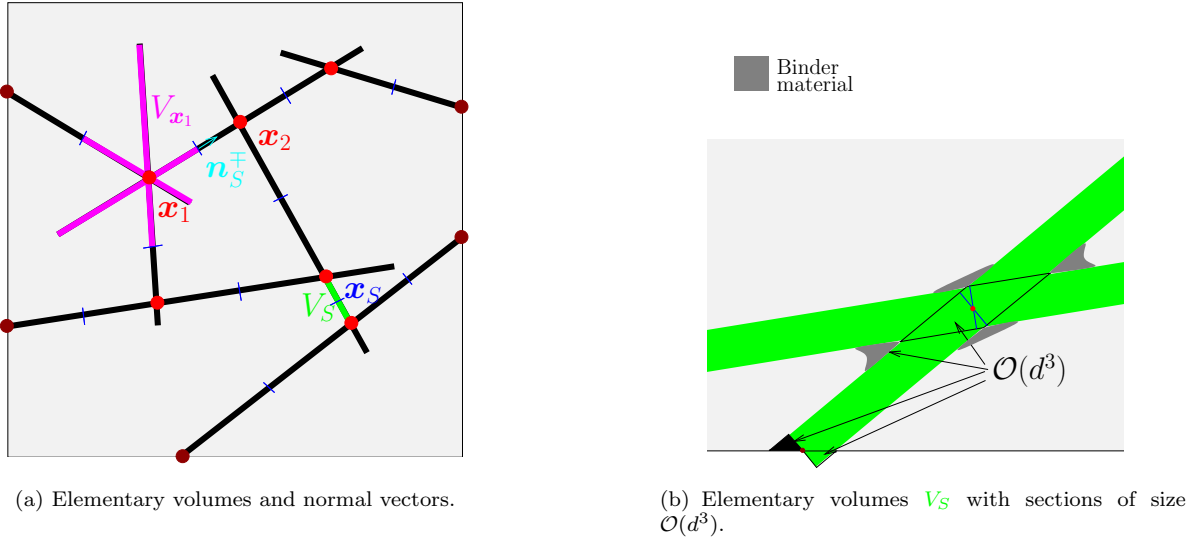


Fig. 5 Interior and boundary nodes for a regular fiber structure.



**Fig. 6** Over-all (a) and zoomed-in (b) sketches of fibrous structures.

**Definition 2**

$$\mathcal{G} : \mathcal{U} \rightarrow \mathcal{F}, \text{ with } \mathcal{G}y(\mathbf{x}_S) = \frac{y(\mathbf{x}_S^+) - y(\mathbf{x}_S^-)}{\|\mathbf{x}_S^+ - \mathbf{x}_S^-\|_2} \mathbf{n}_S^\mp \quad \forall \mathbf{x}_S \in \mathcal{S}, \quad (7a)$$

and

$$\mathcal{D} : \mathcal{F} \rightarrow \mathcal{U}, \text{ with } \mathcal{D}\chi(\mathbf{x}) = \frac{1}{|V_{\mathbf{x}}|} \sum_{\mathbf{x}_S \in \mathcal{S}_{\mathbf{x}}} \chi(\mathbf{x}_S) \cdot \mathbf{n}_S |S| \quad \forall \mathbf{x} \in \bar{\omega}, \quad (7b)$$

where  $\mathbf{n}_S$  is the unit normal vector to  $S$  pointing outside of  $V_{\mathbf{x}}$ .

Finally, we define the following scalar products on  $\mathcal{U}$  and  $\mathcal{F}$ .

**Definition 3**

$$(y, v)_{\mathcal{U}} = \sum_{\mathbf{x} \in \bar{\omega}} |V_{\mathbf{x}}| y(\mathbf{x}) v(\mathbf{x}), \quad (8a)$$

$$(\chi, \tilde{\chi})_{\mathcal{F}} = \sum_{\mathbf{x}_S \in \mathcal{S}} |V_S| (\chi(\mathbf{x}_S) \cdot \mathbf{n}_S) (\tilde{\chi}(\mathbf{x}_S) \cdot \mathbf{n}_S). \quad (8b)$$

As usual, we denote the norms induced by these scalar products by  $\|\cdot\|_{\mathcal{U}}$  and  $\|\cdot\|_{\mathcal{F}}$ , respectively.

### 3 Discretization of the Problem and Error Estimates

We first state an important property of the difference operators  $\mathcal{G}$  and  $\mathcal{D}$ , which is a discrete analog of the equality  $(v, \nabla \cdot \chi) = (\nabla v, \chi)$  valid for any two smooth functions  $v$  and  $\chi$  with a compact support in  $\Omega$  (here  $(\cdot, \cdot)$  is the  $L^2$ -inner product).

**Lemma 1** For all  $y \in \mathcal{U}$  and  $\chi \in \mathcal{F}$

$$(y, \mathcal{D}\chi)_{\mathcal{U}} = -(\mathcal{G}y, \chi)_{\mathcal{F}}. \quad (9)$$

*Proof* Observe, that

$$\begin{aligned} (y, \mathcal{D}\chi)_{\mathcal{U}} &= \sum_{\mathbf{x} \in \bar{\omega}} |V_{\mathbf{x}}| y(\mathbf{x}) \frac{1}{|V_{\mathbf{x}}|} \sum_{\mathbf{x}_S \in \mathcal{S}_{\mathbf{x}}} \chi(\mathbf{x}_S) \cdot \mathbf{n}_S |S| \\ &= \sum_{\mathbf{x} \in \bar{\omega}} \sum_{\mathbf{x}_S \in \mathcal{S}_{\mathbf{x}}} y(\mathbf{x}) \chi(\mathbf{x}_S) \cdot \mathbf{n}_S |S| \\ &= \sum_{\mathbf{x}_S \in \mathcal{S}} \chi(\mathbf{x}_S) \cdot \mathbf{n}_S^\mp (y(\mathbf{x}_S^-) - y(\mathbf{x}_S^+)) |S|, \end{aligned} \quad (10)$$

where the last equality follows from the fact, that each  $\mathbf{x}_S \in \mathcal{S}$  is summed over exactly twice (once for each node on either side of  $S$ ). On the other hand we have

$$\begin{aligned} -(\mathcal{G}y, \chi)_{\mathcal{F}} &= -\sum_{\mathbf{x}_S \in \mathcal{S}} |V_S| (\chi(\mathbf{x}_S) \cdot \mathbf{n}_S) \left( \frac{y(\mathbf{x}_S^+) - y(\mathbf{x}_S^-)}{\|\mathbf{x}_S^- - \mathbf{x}_S^+\|_2} \mathbf{n}_S^\mp \cdot \mathbf{n}_S \right) \\ &= -\sum_{\mathbf{x}_S \in \mathcal{S}} |S| (\chi(\mathbf{x}_S) \cdot \mathbf{n}_S) \mathbf{n}_S \cdot \mathbf{n}_S^\mp (y(\mathbf{x}_S^+) - y(\mathbf{x}_S^-)) \\ &= \sum_{\mathbf{x}_S \in \mathcal{S}} \chi(\mathbf{x}_S) \cdot \mathbf{n}_S^\mp (y(\mathbf{x}_S^-) - y(\mathbf{x}_S^+)) |S|, \end{aligned} \quad (11)$$

where to obtain the second equality we have used that  $|V_S| = |S| \|\mathbf{x}_S^- - \mathbf{x}_S^+\|_2$ , which holds by construction.

Combining (10) and (11) we obtain our claim.

**Definition 4** For  $y \in \mathcal{U}$  define

$$|y|_{\mathcal{G}}^2 := (\mathcal{G}y, \mathcal{G}y)_{\mathcal{F}}. \quad (12)$$

It is easy to see, that  $|\cdot|_{\mathcal{G}}$  defines a semi-norm on  $\mathcal{U}$ . In fact, the semi-norm  $|\cdot|_{\mathcal{G}}$  is a norm on the set  $\{y \in \mathcal{U} \mid y|_{\partial\omega} \equiv 0\}$ . Indeed, we can easily verify that  $|y|_{\mathcal{G}} = 0$  implies  $y \equiv 0$ . By the definition of  $|\cdot|_{\mathcal{G}}$  we have

$$0 = |y|_{\mathcal{G}}^2 = \sum_{\mathbf{x}_S \in \mathcal{S}} |S| \frac{1}{2\|\mathbf{x}_S^+ - \mathbf{x}_S^-\|_2} (y(\mathbf{x}_S^+) - y(\mathbf{x}_S^-))^2.$$

Thus,  $y(\mathbf{x}_S^+) = y(\mathbf{x}_S^-)$  for all  $\mathbf{x}_S \in \mathcal{S}$ , which implies that  $y$  is constant on each subset of  $\bar{\omega}$  corresponding to a path-connected component of  $\Omega_M$ . Since  $y|_{\partial\omega} \equiv 0$  we get that  $y \equiv 0$  in  $\bar{\omega}$  (each path-connected component of  $\Omega_M$  touches  $\partial\Omega$  by assumption).

Now we formulate the finite difference approximation of (4): Find  $y_i \in \mathcal{U}$ ,  $i = 1, 2, 3$  such that

$$\mathcal{D}(K\mathcal{G}y_i) = 0 \quad \text{in } \omega, \quad y_i = x_i \quad \text{on } \partial\omega. \quad (13)$$

**Proposition 1** For  $i = 1, 2, 3$  let  $v_i \in H^1(\Omega_M)$  be the solutions of (4) and let  $y_i$  be the solutions of (13). Then

$$|y_i - v_i|_{\mathcal{G}} \leq \|\boldsymbol{\eta}_i\|_{\mathcal{F}} \quad (14)$$

where the local truncation error  $\boldsymbol{\eta}_i = \boldsymbol{\eta}_i(\mathbf{x}_S)$ ,  $\mathbf{x}_S \in \mathcal{S}$  has the following expression

$$\boldsymbol{\eta}_i(\mathbf{x}_S) = \frac{v_i(\mathbf{x}_S^+) - v_i(\mathbf{x}_S^-)}{\|\mathbf{x}_S^- - \mathbf{x}_S^+\|_2} \mathbf{n}_S^\mp - \frac{1}{|S|} \int_S \nabla v_i dS. \quad (15)$$

*Proof* For any  $\mathbf{x} \in \bar{\omega}$  integrating the first equation of (4) over  $V_{\mathbf{x}}$  and then dividing by  $|V_{\mathbf{x}}|$  we get

$$0 = \frac{1}{|V_{\mathbf{x}}|} \int_{V_{\mathbf{x}}} \Delta v_i d\mathbf{x} = \frac{1}{|V_{\mathbf{x}}|} \left( \sum_{\mathbf{x}_S \in \mathcal{S}_{\mathbf{x}}} \int_S \nabla v_i dS \cdot \mathbf{n}_S + \int_{\partial V_{\mathbf{x}} \cap \partial\Omega} \nabla v_i dS \cdot \mathbf{n}_{\Omega} \right) = \mathcal{D}\tilde{\boldsymbol{\eta}}_i(\mathbf{x}) + \boldsymbol{\eta}_i^*(\mathbf{x}),$$

with  $\tilde{\boldsymbol{\eta}}_i(\mathbf{x}_S) = \frac{1}{|S|} \int_S \nabla v_i dS$  and  $\boldsymbol{\eta}_i^*(\mathbf{x}) = \frac{1}{|V_{\mathbf{x}}|} \int_{\partial V_{\mathbf{x}} \cap \partial\Omega} \nabla v_i dS \cdot \mathbf{n}_{\Omega}$ , where  $\mathbf{n}_{\Omega}$  is the outer unit normal vector to  $\partial\Omega$ . Note, that  $\boldsymbol{\eta}_i^*(\mathbf{x}) = 0$  for  $\mathbf{x} \in \omega$ . Since  $v_i - y_i = 0$  on  $\partial\omega$  we thus obtain

$$\begin{aligned} (\mathcal{G}(v_i - y_i), \mathcal{G}(v_i - y_i))_{\mathcal{F}} &= -(\mathcal{D}(\mathcal{G}v_i), v_i - y_i)_{\mathcal{U}} = -(\mathcal{D}(\mathcal{G}v_i - \tilde{\boldsymbol{\eta}}_i) - \boldsymbol{\eta}_i^*, v_i - y_i)_{\mathcal{U}} \\ &= -(\mathcal{D}(\mathcal{G}v_i - \tilde{\boldsymbol{\eta}}_i), v_i - y_i)_{\mathcal{U}} = (\boldsymbol{\eta}_i, \mathcal{G}(v_i - y_i))_{\mathcal{F}}. \end{aligned}$$

Here we have used Lemma 1, the definition of  $\boldsymbol{\eta}_i$  by (15), and the definition of  $\mathcal{G}v_i$  by (7a). Now applying Schwarz inequality for the right hand side we get the desired result (14).

Now we can give an approximation  $\tilde{K}^G$  to the upscaled thermal conductivity tensor  $\tilde{K}$  (here  $G$  refers to “graph”). Let  $y_i$ ,  $i = 1, 2, 3$  be the solutions of the discrete problems (13). Then

$$\tilde{K}^G e_i := \frac{1}{|\Omega|} \sum_{\mathbf{x}_S \in \mathcal{S}} \mathcal{G}y_i(\mathbf{x}_S) |V_S|. \quad (16)$$

We are now ready to state the final result regarding the error analysis.

**Proposition 2** Let  $y_i$ ,  $i = 1, 2, 3$  be solutions of (13) and let the approximate upscaled conductivity tensor  $\tilde{K}^G$  be defined by (16). Then

$$\|\tilde{K} - \tilde{K}^G\| \leq C(\delta + \|\boldsymbol{\eta}\|_{\mathcal{F}} + \|\Psi\|), \quad (17)$$

where  $\|\cdot\|$  is some matrix norm,  $\boldsymbol{\eta} := [\eta_i]_{i=1}^3$  with  $\|\boldsymbol{\eta}\|_{\mathcal{F}} := \max_i \|\eta_i\|_{\mathcal{F}}$ , and the approximation error  $\Psi$  is a  $3 \times 3$  matrix with the  $i$ -th column given by

$$\boldsymbol{\psi}_i = \frac{1}{|\Omega|} \left( \int_{\Omega_M} \nabla v_i d\mathbf{x} - \sum_{\mathbf{x}_S \in \mathcal{S}} \mathcal{G}v_i(\mathbf{x}_S) |V_S| \right). \quad (18)$$

*Proof* Note, that by (3) and using the definition of  $\boldsymbol{\psi}_i$  we have

$$\begin{aligned} \tilde{K}\mathbf{e}_i - \tilde{K}^G\mathbf{e}_i &= \frac{1}{|\Omega|} \int_{\Omega_M} \nabla v_i d\mathbf{x} - \frac{1}{|\Omega|} \sum_{\mathbf{x}_S \in \mathcal{S}} \mathcal{G}y_i(\mathbf{x}_S) |V_S| + \mathcal{O}(\delta) \\ &= \boldsymbol{\psi}_i + \frac{1}{|\Omega|} \sum_{\mathbf{x}_S \in \mathcal{S}} \mathcal{G}(v_i - y_i)(\mathbf{x}_S) |V_S| + \mathcal{O}(\delta). \end{aligned}$$

Thus, taking the Euclidean vector norm and using the Cauchy-Schwarz inequality we have

$$\begin{aligned} \|(\tilde{K} - \tilde{K}^G)\mathbf{e}_i\|_2 &\leq \|\boldsymbol{\psi}_i\|_2 + \frac{1}{|\Omega|} \sum_{\mathbf{x}_S \in \mathcal{S}} \|\mathcal{G}(v_i - y_i)(\mathbf{x}_S)\|_2 |V_S| + \mathcal{O}(\delta) \\ &\leq \|\boldsymbol{\psi}_i\|_2 + \frac{1}{|\Omega|} \left( \sum_{\mathbf{x}_S \in \mathcal{S}} |V_S| \right)^{\frac{1}{2}} \left( \sum_{\mathbf{x}_S \in \mathcal{S}} \|\mathcal{G}(v_i - y_i)(\mathbf{x}_S)\|_2^2 |V_S| \right)^{\frac{1}{2}} + \mathcal{O}(\delta). \end{aligned}$$

Then (14) yields

$$\|\boldsymbol{\eta}_i\|_{\mathcal{F}}^2 \geq \sum_{\mathbf{x}_S \in \mathcal{S}} |V_S| (\mathcal{G}(y_i - v_i)(\mathbf{x}_S) \cdot \mathbf{n}_S)^2 = \sum_{\mathbf{x}_S \in \mathcal{S}} |V_S| \|\mathcal{G}(y_i - v_i)(\mathbf{x}_S)\|_2^2.$$

Combining the last two results we arrive at

$$\|(\tilde{K} - \tilde{K}^G)\mathbf{e}_i\|_2 \leq \|\boldsymbol{\psi}_i\|_2 + C\|\boldsymbol{\eta}_i\|_{\mathcal{F}} + \mathcal{O}(\delta)$$

from where we easily deduce (17) using the equivalence of norms.

To make the estimate (17) practically useful we need to bound the terms of the local truncation error  $\boldsymbol{\eta}$  and the approximation error  $\Psi$ . Given the complexity of the fiber structures that we would like to treat it would be very difficult to derive any mathematically rigorous bounds. However, we can make several important observations (cf., e.g. [13]).

By (15) we have that for a fixed  $\mathbf{x}_S \in \mathcal{S}$

$$\boldsymbol{\eta}_i(\mathbf{x}_S) \cdot \mathbf{n}_S^{\mp} = \frac{v_i(\mathbf{x}_S^+) - v_i(\mathbf{x}_S^-)}{\|\mathbf{x}_S^- - \mathbf{x}_S^+\|_2} - \frac{1}{|S|} \int_S \nabla v_i dS \cdot \mathbf{n}_S^{\mp}. \quad (19)$$

Without loss of generality we may assume that

$$\mathbf{x}_S = \mathbf{0}, \mathbf{n}_S^{\mp} = \mathbf{e}_1, \|\mathbf{x}_S^+ - \mathbf{x}_S^-\|_2 = h, \text{ and } \text{diam}(S) = d, \quad (20)$$

so that  $S = \{(0, x_2, x_3) : x_2^2 + x_3^2 \leq d^2/4\}$ . Thus, (19) simplyfies to

$$\boldsymbol{\eta}_i(\mathbf{x}_S) \cdot \mathbf{n}_S^{\mp} = \frac{1}{h} \int_{-h/2}^{h/2} \frac{\partial v_i}{\partial x_1}(x_1, 0, 0) dx_1 - \frac{1}{|S|} \int_S \frac{\partial v_i}{\partial x_1} dS.$$

Now, with  $\tilde{\mathbf{x}} = (\tilde{x}_1, \tilde{x}_2, \tilde{x}_3) := (\frac{x_1}{h}, \frac{x_2}{d}, \frac{x_3}{d})$  and  $\tilde{v}_i(\tilde{\mathbf{x}}) := v_i(\mathbf{x})$  we obtain the scaled equation

$$\boldsymbol{\eta}_i(\mathbf{x}_S) \cdot \mathbf{n}_S^{\mp} = \frac{1}{h} \left( \int_{-1/2}^{1/2} \frac{\partial \tilde{v}_i}{\partial \tilde{x}_1}(\tilde{x}_1, 0, 0) d\tilde{x}_1 - \frac{1}{|\tilde{S}|} \int_{\tilde{S}} \frac{\partial \tilde{v}_i}{\partial \tilde{x}_1} d\tilde{S} \right), \quad (21)$$

where  $\tilde{S}$  is the scaled cross-section corresponding to  $S$  (scaled by  $1/d$  in  $x_2$  and  $x_3$ ). It is straightforward to verify that the right hand side of (21) defines a linear functional for  $\frac{\partial \tilde{v}_i}{\partial \tilde{x}_1}$  which vanishes for all polynomials with degree at most 1. Hence, applying the Bramble-Hilbert lemma we obtain

$$|\boldsymbol{\eta}_i(\mathbf{x}_S) \cdot \mathbf{n}_S^\mp| \leq \frac{C}{h} \left| \frac{\partial \tilde{v}_i}{\partial \tilde{x}_1} \right|_{H^2(\tilde{V}_S)}, \quad (22)$$

where  $\tilde{V}_S$  is the scaled volume corresponding to  $V_S$  (scaled by  $1/h$  in  $x_1$  and by  $1/d$  in  $x_2$  and  $x_3$ ) and  $C$  is a constant independent of  $h$  and  $d$ . Since

$$\left| \frac{\partial \tilde{v}_i}{\partial \tilde{x}_1} \right|_{H^2(\tilde{V}_S)}^2 = \sum_{|\gamma|=2} \int_{\tilde{V}_S} \left( \frac{\partial^3 \tilde{v}_i}{\partial \tilde{x}_1 \partial \tilde{\mathbf{x}}^\gamma} \right)^2 d\tilde{\mathbf{x}},$$

where  $\gamma = (\gamma_1, \gamma_2, \gamma_3)$  is a multi-index, and noting that  $\frac{\partial^3 \tilde{v}_i}{\partial \tilde{x}_1 \partial \tilde{\mathbf{x}}^\gamma} = h^{\gamma_1+1} d^{\gamma_2+\gamma_3} \frac{\partial^3 v_i}{\partial x_1 \partial \mathbf{x}^\gamma}$  we obtain

$$|\boldsymbol{\eta}_i(\mathbf{x}_S) \cdot \mathbf{n}_S^\mp| \leq \frac{C}{h} \left( \frac{1}{|V_S|} \sum_{|\gamma|=2} h^{2(\gamma_1+1)} d^{2(\gamma_2+\gamma_3)} \int_{V_S} \left( \frac{\partial^3 v_i}{\partial x_1 \partial \mathbf{x}^\gamma} \right)^2 d\mathbf{x} \right)^{\frac{1}{2}}$$

after a coordinate transform from  $\tilde{\mathbf{x}}$  to  $\mathbf{x}$ . With this in mind we have

$$\|\boldsymbol{\eta}_i\|_{\mathcal{F}}^2 = \sum_{\mathbf{x}_S \in \mathcal{S}} |V_S| (\boldsymbol{\eta}_i(\mathbf{x}_S) \cdot \mathbf{n}_S)^2 \leq C \sum_{|\gamma|=2} h^{2\gamma_1} d^{2(\gamma_2+\gamma_3)} \int_{V_S} \left( \frac{\partial^3 v_i}{\partial x_1 \partial \mathbf{x}^\gamma} \right)^2 d\mathbf{x}$$

Under the condition that the third derivatives of  $v_i$  are bounded independently of  $d$  and  $h$  we thus have

$$\|\boldsymbol{\eta}_i\|_{\mathcal{F}} = \mathcal{O}(h^2 + dh + d^2) \quad (23)$$

Similar arguments can be made in estimating the other term  $\Psi$ . Again assuming (20) we have that

$$\begin{aligned} \int_{V_S} \nabla v_i d\mathbf{x} - \mathcal{G} v_i(\mathbf{x}_S) |V_S| &= \int_{V_S} \nabla v_i d\mathbf{x} - \mathcal{G} v_i(\mathbf{x}_S) |V_S| \\ &- \frac{|V_S|}{2} \left[ \left( \frac{\partial v_i}{\partial x_2}(0, \frac{d}{2}, 0) + \frac{\partial v_i}{\partial x_2}(0, -\frac{d}{2}, 0) \right) e_2 + \left( \frac{\partial v_i}{\partial x_3}(0, 0, \frac{d}{2}) + \frac{\partial v_i}{\partial x_3}(0, 0, -\frac{d}{2}) \right) e_3 \right], \end{aligned} \quad (24)$$

where the last term vanishes due to the boundary conditions in (4). It is straightforward to verify that the right hand side of (24) defines a linear functional, which vanishes for all polynomials  $v_i$  with degree at most 2. Thus, by a scaling argument completely analogous to the one above and by the Bramble-Hilbert lemma we can bound the left hand side of (24) by the  $H^3(V_S)$  semi-norm of  $v_i$  and powers of  $h$  and  $d$ , where all involved terms are of higher order than in estimate (23).

Now, note that by Assumption 2 we have

$$\int_{\Omega_M} \nabla v_i d\mathbf{x} = \sum_{\mathbf{x}_S \in \mathcal{S}} \int_{V_S} \nabla v_i d\mathbf{x} + \mathcal{O}\left(\frac{d^3}{h^3}\right).$$

Summation over  $\mathbf{x}_S \in \mathcal{S}$  and noting that  $2hd \leq h^2 + d^2$  thus yields the estimate

$$\|\tilde{K} - \tilde{K}^G\| = \mathcal{O}\left(h^2 + d^2 + \frac{d^3}{h^3} + \delta\right). \quad (25)$$

To make this formal error estimate mathematically rigorous, we, however, need to prove bounds for the third derivatives of the solution  $v_i$  independently of  $h$  and  $d$ . Theoretically, this could be done by asymptotic expansion of the solution with respect to the small parameter  $\frac{d}{h}$  and proving certain bounds for the terms of the expansion. However, in the generality of our setting with a complex structure of the fiber material, multiple diameter sizes, and the presence of binder material that rounds the corners of the fiber interfaces, this is a very difficult task, which is beyond the scope of this paper.

Our aim is to experimentally study and test the accuracy of the proposed method. In accordance with the derivations above we take estimate (25) as a working hypothesis for our numerical and experimental study.

#### 4 Numerical Results and Conclusions

We specify the components of the algorithm we have used in the computations:

First we determine all crossings of fibers and construct an undirected graph. If this is done straightforwardly by checking each fiber for intersection with any other, the numerical complexity of this procedure is quadratic in the total number of fibers, i.e.  $\mathcal{O}(n_\phi^2)$ , where  $n_\phi$  is the total number of fibers. In [3] it is discussed how this can be reduced to a complexity which is  $\mathcal{O}(n_\phi^{3/2})$  by a domain decomposition approach. Having obtained the graph we set up the discrete system defined by (13), which is then solved by the ILU preconditioned Conjugate Gradient method implemented in the LASPack package<sup>2</sup>. The solution is post-processed according to (16) to compute the effective thermal conductivity.

As noted in [6, section 4], the flux in  $\Omega_A$  and in the path-connected components of  $\Omega_M$  which do not touch  $\partial\Omega$  are not used in the computations. Asymptotically, as  $\delta \rightarrow 0$  these components can be neglected. Nonetheless, for a specific choice for  $\delta$  we may still hope to (and in many numerically tested cases do) obtain better approximations of the effective thermal conductivities, by taking into account some approximation of the flux in those regions. This is in particular true for materials with a (very) low solid volume fraction for which  $|\Omega_M|/|\Omega|$  and  $\delta$  are of the same order. In the numerical examples presented below the temperature in  $\Omega_A$  is approximated by linearly interpolating the (Dirichlet) boundary conditions, leading to a constant temperature gradient. The temperature gradient in the path-connected components of  $\Omega_M$  that do not touch the boundary is obtained in the same way and then scaled by  $\delta$  (see [6]). The actual quantity produced by our algorithm is thus given by

$$\tilde{K}^{G+A} := \tilde{K}^G + \frac{|\Omega_A|}{|\Omega|} \delta I,$$

where  $I$  is the identity matrix in  $\mathbb{R}^3$  and  $A$  stands for ‘‘air’’. We call the resulting solver ‘‘COGraph’’.

In the numerical experiments we first test the validity the main estimate of this paper, i.e. (25). Note, that in (25) we have four error terms, i.e.  $\mathcal{O}(d^2)$ ,  $\mathcal{O}(h^2)$ ,  $\mathcal{O}((d/h)^3)$ , and  $\mathcal{O}(\delta)$ . Apparently, it is rather hard to analyze all of these error terms independently of each other, in particular since three of them simultaneously depend on the quantities  $d$  and  $h$ . On the other hand the  $\mathcal{O}(\delta)$ -term can be taken out completely, if in (25) we replace  $\tilde{K}\mathbf{e}_i$  by  $(\int_{\Omega_M} \nabla v_i d\mathbf{x} + |\Omega_A|\delta\mathbf{e}_i)/|\Omega|$  (see (3) and [6, equation (4.3)]). Thus, we can isolate the error depending on the geometric quantities  $d$  and  $h$  from the error related to the contrast  $\delta$ . In the computations below we compare  $\tilde{K}^{G+A}$  with the quantity produced by [6, Algorithm 2] and denoted by  $\tilde{K}^{CO+A}$ . Note, that this is equivalent to (25) up to some (discretization) error, which is certainly introduced by replacing  $(\int_{\Omega_M} K \nabla v_i d\mathbf{x} + |\Omega_A|\delta\mathbf{e}_i)/|\Omega|$  with  $\tilde{K}^{CO+A}\mathbf{e}_i$ .

Now, we consider a series of randomly generated geometries. The parameters  $d$ ,  $h$ , and  $d/h$  are chosen in such way that they decrease simultaneously. (Here we have taken  $h$  to be the arithmetic mean of all edges in the graph.) For all geometries we choose  $\delta = 0.02$ , which corresponds to a contrast typical of industrial materials like glass or mineral wool. In Figures 7-9 we show the results of the computations. Since the relative error is often more interesting than the absolute one, we also report  $\max_{i,j} |(\tilde{K}_{i,j}^{CO+A} - \tilde{K}_{i,j}^{G+A})/\tilde{K}_{j,j}^{CO+A}|$ . For the sake of completeness we also provide the computed effective thermal conductivity along with some additional information about the geometries in Table 1. We report only the diagonal entries, since they are by orders of magnitude larger than the off-diagonal entries.

<sup>2</sup> For more details we refer to [www.mgnet.org/mgnet/Codes/laspak/html/laspak.html](http://www.mgnet.org/mgnet/Codes/laspak/html/laspak.html)

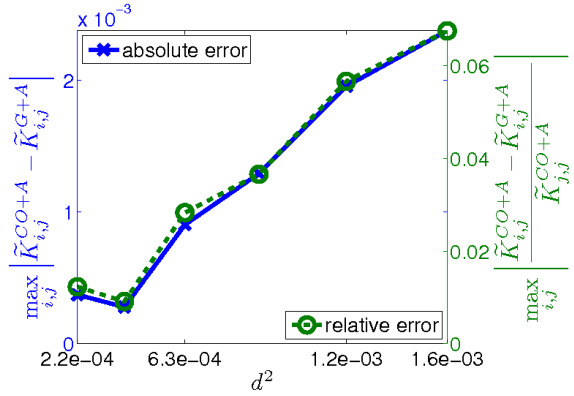
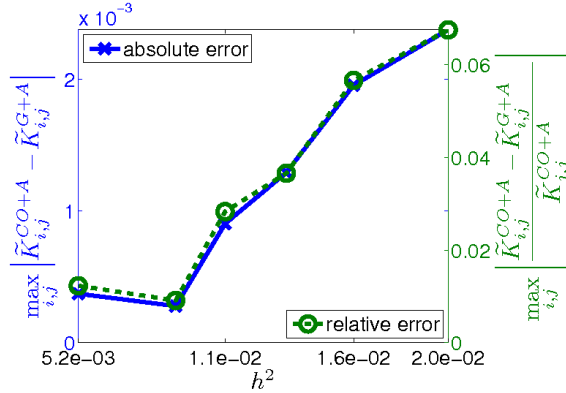


Fig. 7 Error vs. characteristic fiber diameter.



**Fig. 8** Error vs. characteristic edge length.

Examining the graphs shown in Figures 7-9 and the data of Table 1 we see that at first, as  $d$  decreases, the error decreases linearly in  $d^2$ . This is in accordance with the developed theory. However, for the last geometry, when  $d$  becomes very small, we see that the difference between our computations and [6, equation (4.3)] increases. This behavior could be caused by an increase in the norm of the third derivatives of  $v_i$  affecting estimate (25). However, it may also be attributed to the fact that for the last geometry the voxelized discretization used to compute  $\tilde{K}^{CO+A}$  introduces a discretization error which over-compensates the error reduction due to the decrease in  $d$ ,  $h$ , and  $d/h$ . More specifically, for all geometries treated in Figures 7-9 and Table 1 we have used a  $400^3$ -mesh for the discretization to compute  $\tilde{K}^{CO+A}$ . Due to the rescaling to the unit cube this means that  $d = 0.04$  corresponds to 16 voxels but  $d = 0.015$  to only 6 voxels. It is quite obvious that the approximation of a cylinder by voxels whose side lengths are only  $\frac{1}{6}$  the size of the cylinder's diameter cannot be very accurate. Certainly, with such a poor approximation of the geometry we cannot expect to get a very accurate approximation of the solution of (4). Unfortunately, we are not able to consider finer meshes to validate this explanation, since this would result in too high a number of unknowns in the calculation of  $\tilde{K}^{CO+A}$  (cf. [6, Algorithm 2]).

Also, we note that the relative error has essentially the same behavior (on a different scale) as the absolute one. Overall, we consider the quality of the approximation provided by  $\tilde{K}^{G+A}$  quite satisfactory.

Now we consider two different geometries, for which we compare the performance of the proposed method with a commercially available software. The fiber structures have a solid volume fraction of 5%, i.e.  $|\Omega_M|/|\Omega| = 0.05$ , (see Figure 10(a)) and 15%, i.e.  $|\Omega_M|/|\Omega| = 0.15$ , (see Figure 10(b)), respectively. In both cases 80% of the fiber volume is occupied by long thin fibers (colored white), whereas the remaining 20% are taken up by short thick fibers (colored red). Both fiber materials are isotropic. The data is generated by GeoDict using a  $500^3$  voxel mesh for discretization.

Now, we compare the effective thermal conductivity tensors of these two structures computed by GeoDict, which in turn uses the solver EJ-HEAT (cf. [17]), with  $\tilde{K}^{G+A}$ . Note, that GeoDict uses periodic boundary conditions in the formulation of the cell problems, whereas we use linear boundary conditions. It is well known (cf. e.g. [2]), that for REVs these different types of boundary conditions produce (asymptotically with respect to the length scale of the microscopic variations) the same effective conductivity tensors. Again we set  $\delta = 0.02$ . Using the analysis of [9] it is reasonable to assume, that for this contrast both fiber geometries constitute REVs. Tables 2(a) and 2(b) show the numerical results produced by GeoDict and our method, respectively. As stopping criterion we use a relative accuracy of  $1e-6$  in all cases. For comparing the efficiency, we also report the total runtime of each algorithm and the used memory. Again we report

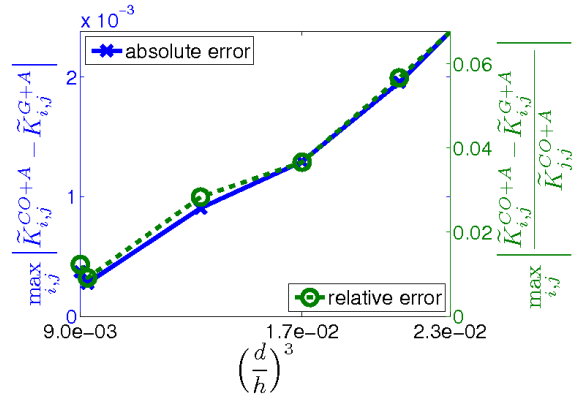


**Fig. 9** Error vs. ratio of characteristic diameter and edge length.

	$\tilde{K}^{G+A}$	$\tilde{K}^{CO+A}$
$d = 4.00e-02$ $h = 1.41e-01$ $\frac{d}{h} = 2.84e-01$ SVP: 5%	<b>4.00e-02</b> - <b>3.52e-02</b> -   - <b>3.28e-02</b>	<b>4.15e-02</b> -   - <b>3.71e-02</b> -   - <b>3.52e-02</b>
$d = 3.50e-02$ $h = 1.27e-01$ $\frac{d}{h} = 2.76e-01$ SVP: 5%	<b>3.94e-02</b> -   - <b>3.25e-02</b> -   - <b>3.58e-02</b>	<b>4.03e-02</b> -   - <b>3.45e-02</b> -   - <b>3.71e-02</b>
$d = 3.00e-02$ $h = 1.16e-01$ $\frac{d}{h} = 2.59e-01$ SVP: 4.5%	<b>3.50e-02</b> -   - <b>3.40e-02</b> -   - <b>3.41e-02</b>	<b>3.60e-02</b> -   - <b>3.53e-02</b> -   - <b>3.52e-02</b>
$d = 2.50e-02$ $h = 1.05e-01$ $\frac{d}{h} = 2.38e-01$ SVP: 4%	<b>3.40e-02</b> -   - <b>3.10e-02</b> -   - <b>3.33e-02</b>	<b>3.45e-02</b> -   - <b>3.19e-02</b> -   - <b>3.38e-02</b>
$d = 2.00e-02$ $h = 9.52e-02$ $\frac{d}{h} = 2.10e-01$ SVP: 3.5%	<b>3.13e-02</b> -   - <b>3.17e-02</b> -   - <b>3.02e-02</b>	<b>3.15e-02</b> -   - <b>3.19e-02</b> -   - <b>3.05e-02</b>
$d = 1.50e-02$ $h = 7.21e-02$ $\frac{d}{h} = 2.08e-01$ SVP: 3%	<b>2.89e-02</b> -   - <b>3.06e-02</b> -   - <b>2.89e-02</b>	<b>2.87e-02</b> -   - <b>3.02e-02</b> -   - <b>2.88e-02</b>

**Table 1** Main diagonals of effective thermal conductivity tensors for a series of geometries with decreasing  $d$ ,  $h$ , and  $\frac{d}{h}$ . The solid volume percentage (SVP), i.e. the volumetric fiber content, is also reported for each geometry.

only the diagonal elements of the effective thermal conductivity tensors. For an objective comparison all computations were performed on the same computer platform.

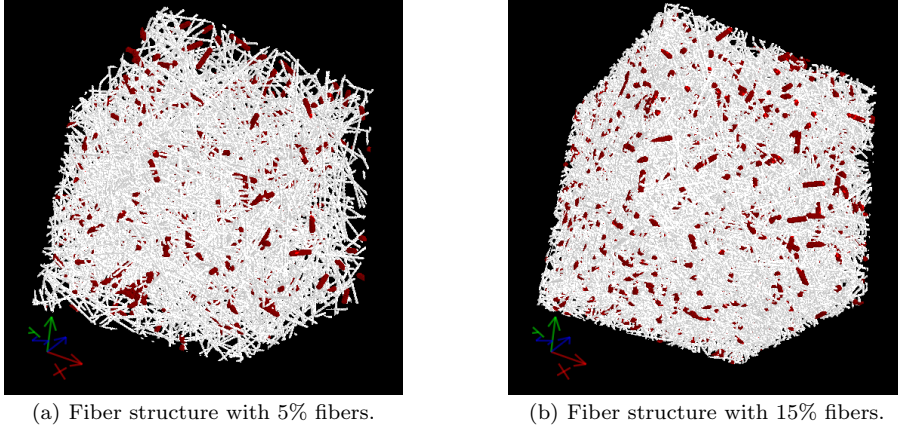


**Fig. 10** Two fiber structures with different densities of fibers.

Table 2 shows that the conductivity tensors produced by COGraph and GeoDict are comparable. Comparing the required runtime and the used memory, however, we see, that COGraph uses significantly fewer resources. For the geometry containing only 5% fiber material it requires less than 0.02% of the time and about 0.4% of the memory that is required by the EJ-HEAT solver. For the denser fiber geometry these differences aren't quite as large, however, they remain substantial.

It is obvious, that increasing the number of fibers, while keeping the size and resolution of the voxelized gird constant, affects the performance of COGraph more than that of GeoDict. The reason is, that more fibers usually have more intersections entailing a higher number of unknowns for COGraph, while the

(a) Effective thermal conductivity tensor of the fiber structure shown in 10(a).

	$\tilde{K}^{GeoDict}$	$\tilde{K}^{G+A}$
	<b>3.31e-2</b> - - -	<b>3.34e-2</b> - - -
# unknowns	- <b>3.27e-2</b> - <b>3.23e-2</b> 1.25e8	- <b>3.29e-2</b> - <b>3.25e-2</b> 3859
runtime	- -> 5500sec.	< 1sec.
memory	- 3169MB	<b>13MB</b>

(b) Effective thermal conductivity tensor of the fiber structure shown in 10(b).

	$\tilde{K}^{GeoDict}$	$\tilde{K}^{G+A}$
	<b>6.49e-2</b> - - -	<b>6.32e-2</b> - - -
# unknowns	- <b>6.38e-2</b> - <b>6.55e-2</b> 1.25e8	- <b>6.19e-2</b> - <b>6.41e-2</b> 26549
runtime	- -> 6000sec.	< 5sec.
memory	- 4876MB	<b>84MB</b>

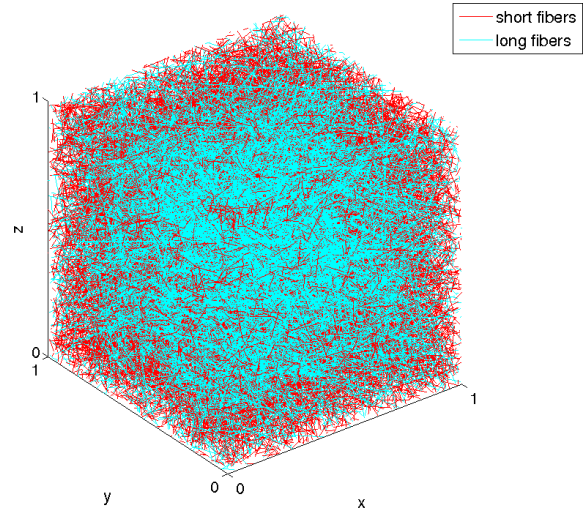
**Table 2** Comparison of the effective thermal conductivity tensors for the fiber structures shown in Figure 10 computed by GeoDict and COGraph.  $\delta = 0.02$ .

number of unknowns for EJ-HEAT stays exactly the same. Nonetheless, the number of unknowns for COGraph remains several orders of magnitude smaller than that of EJ-HEAT.

These observations also concern a related issue. For a geometry where only a (very) small fraction of the total volume is occupied by fibers we typically need a (very) large sample size to obtain an REV (cf. [9]). For some glass- and mineral-wool materials the solid volume fraction is less than 1%. In order to resolve the fibers of such a structure in a large enough sample, one needs to consider voxel discretizations with  $1000^3$ ,  $2000^3$ , or even more unknowns depending on the remaining material parameters, such as fiber thickness, conductivity of the fiber material, etc. To solve a cell problem on such a fine grid with a standard software can easily become prohibitively expensive. COGraph, on the other hand, is only sensitive to the number of fiber intersections, which is related to the total number of fibers and thus to the total amount of fiber

material in a sample. Due to this property COGraph is particularly well suited for calculating the effective thermal conductivity tensors for large sparse fiber geometries. As an example for such a large sparse fiber geometry we refer to Figure 11. This structure consisting of 35830 fibers has a solid volume fraction of 1% and is discretized by  $2000^3$  voxels. 50% of the highly conductive material is occupied by short fibers, which are 100 voxels long, and the rest is occupied by long fibers ranging from one side of the sample to another one. For this geometry our algorithm needs 95 seconds to compute  $\tilde{K}^{G+A}$ . By the domain decomposition approach discussed in [3] for constructing the graph this time can be further reduced to 2 seconds. This again exemplifies the efficiency and competitiveness of our method.

In conclusion, we have developed an algorithm that can be used as a specialized tool for computing the effective thermal conductivity tensors of high contrast fibrous materials. For fiber structures with a (very) low solid-volume-fraction it allows to consider (very) large sample sizes, which are often too large to be treated by classical methods.

**Fig. 11** Large, sparse fiber geometry with a solid volume fraction of 1% resolved by a  $2000^3$  voxelized mesh.

## Acknowledgments

The research of R. Lazarov was supported in parts by NSF Grant DMS-0713829, by the European School for Industrial Mathematics (ESIM) sponsored by the Erasmus Mundus program of the EU, and by award KUS-C1-016-04, made by King Abdullah University of Science and Technology (KAUST). O. Iliev was supported by DAAD-PPP D/07/10578, and J. Willems was supported by DAAD-PPP D/07/10578 and the Studienstiftung des deutschen Volkes (German National Academic Foundation).

## References

1. G.I. Barenblatt, V.M. Entov, and V.M. Ryzhik. *Movement of Liquids and Gases in Natural Strata*. Nedra, 1984.
2. A. Bourgeat and A. Piatnitski. Approximations of effective coefficients in stochastic homogenization. *Ann. Inst. Henri Poincaré, Probab. Stat.*, 40(2):153–165, 2004.
3. A. Brandt, O. Iliev, and J. Willems. A domain decomposition approach for calculating the graph corresponding to a fibrous geometry. In M. Bercovier, D.E. Keyes, M. Gardner, and O.B. Widlund, editors, *Domain Decomposition Methods in Science and Engineering XVIII*, Lecture Notes in Computational Science and Engineering. Springer, 2009, to appear.
4. G.A. Chechkin, V.V. Jikov, D. Lukkassen, and A.L. Piatnitski. On homogenization of networks and junctions. *Asymptotic Anal.*, 30(1):61–80, 2002.
5. D. Cioranescu and A. El Janati. Mathematical analysis of lattice-type structures with complicated geometry. *Math. Mech. Solids*, 6(1):87–110, 2001.
6. R. Ewing, O. Iliev, R. Lazarov, I. Rybak, and J. Willems. A simplified method for upscaling composite materials with high contrast of the conductivity. *SIAM Journal on Scientific Computing*, to appear.
7. R. Eymard, T. Gallouët, and R. Herbin. Finite Volume Methods. In *Handbook of Numerical Analysis*, Vol. VII, pages 713–1020. North-Holland, Amsterdam, 2000.
8. U. Hornung, editor. *Homogenization and Porous Media*, volume 6 of *Interdisciplinary Applied Mathematics*. Springer, 1st edition, 1997.
9. O. Iliev, I. Rybak, and J. Willems. On upscaling heat conductivity for a class of industrial problems. Technical Report 120, Fraunhofer ITWM, 2007. Submitted to the *Journal of Theoretical and Applied Mechanics*.
10. V. V. Jikov, S. M. Kozlov, and O. A. Oleinik. *Homogenization of Differential Operators and Integral Functionals*. Springer, 1st edition, 1994.
11. G. Panasenko. *Multi-Scale Modelling for Structures and Composites*. Springer, 1st edition, 2005.
12. A. A. Samarskii. *The Theory of Finite Difference Schemes*. Monographs and Textbooks in Pure and Applied Mathematics. Marcel Dekker, New York, 2001.
13. A. A. Samarskii, R. D. Lazarov, and V. L. Makarov. *Finite Difference Schemes for Differential Equations with Generalized Solutions*. Vissaya Shkola, Moscow, 1987.
14. S. Torquato. *Random Heterogeneous Materials. Microstructure and Macroscopic Properties*. Interdisciplinary Applied Mathematics. 16. New York, NY: Springer, 2002.
15. J.-P. Vassal, L. Orgéas, D. Favier, J.-L. Auriault, and S. Le Corre. Upscaling the diffusion equations in particulate media made of highly conductive particles. i. theoretical aspects. *Physical Review E (Statistical, Nonlinear, and Soft Matter Physics)*, 77(1):011302, 2008.
16. J.-P. Vassal, L. Orgéas, D. Favier, J.-L. Auriault, and S. Le Corre. Upscaling the diffusion equations in particulate media made of highly conductive particles. ii. application to fibrous material. *Physical Review E (Statistical, Nonlinear, and Soft Matter Physics)*, 77(1):011303, 2008.
17. A. Wiegmann and A. Zemitzis. EJ-HEAT: A fast explicit jump harmonic averaging solver for the effective heat conductivity of composite materials. Technical Report 94, Fraunhofer-Institut für Techno- und Wirtschaftsmathematik, 2006.
18. X. H. Wu, Y. Efendiev, and T. Y. Hou. Analysis of upscaling absolute permeability. *Discrete Contin. Dyn. Syst., Ser. B*, 2(2):185–204, 2002.